Journal of Intelligent & Robotic Systems (2022) 104: 64
https://doi.org/10.1007/s10846-022-01614-3

REGULAR PAPER

Design and Dynamic Analysis of a Compliant Leg Configuration towards the Biped Robot's Spring-Like Walking

Guifu Luo [1] · Ruilong Du [2,3] · Shiqiang Zhu [2] · Sumian Song [2] · Haihui Yuan [2,3] · Hua Zhou [1] · Mingguo Zhao [3] · Jason Gu [4]

Received: 1 October 2021 / Accepted: 9 March 2022 / Published online: 30 March 2022

Abstract
The spring-loaded inverted pendulum (SLIP) model has been proven successfully applied to implement spring-like walking for biped robots. This work presents a compliant leg configuration that can meet the requirements of the SLIP model. The leg is characterized by the fact that most of the mass is concentrated in the hip, and the leg is spring-like and light in weight. Numerical models were introduced to analyze the stiffness of the leg, and its dynamic characteristics with the mass of the leg being taken into account. Using the proposed model, the analysis on the stiffness showed that the leg could be taken as a variable stiffness spring with respect to the length of the leg, the longer the leg, the greater the stiffness. In addition to this, it suggested that the mass of the leg should be maintained below one-tenth of the mass concentrated in the hip to perform spring-like walking. Experiments regarding the stiffness and dynamic characteristics showed a good agreement with the simulation results, thus verifying the presented leg configuration and the numerical models. Afterwards, experiments were conducted on vertical jumps of the leg, demonstrating the feasibility of the leg to perform the biped's spring-like walking, regardless of being at a certain speed, or at varying speeds.

Keywords Biped robot · Compliant leg configuration · Leg stiffness · Dynamic analysis · Spring-like walking

1 Introduction

Biped robots have demonstrated lots of advantages in communicating with human-built environments due to their human-like configurations [1]. To implement the walking of a biped robot, the two legs are the main parts that touch the ground successively, and therefore, the locomotion behavior of a biped robot would be greatly influenced by its leg configuration. For decades, there has been great interest in developing different types of leg configurations and their related walking mechanisms.

Typically, two main concepts could be found on exploring the walking mechanisms of biped robots. One of them would

Guifu Luo and Ruilong Du contributed equally to this work.

Research supported by NSFC Project (No. 51905495, No.51821093, No.51890885), the China Postdoctoral Project (No. 2020M671821), NSF Project of Zhejiang Province (No. LQ20E050009, No. LQ21F030003), and the National Key Research and Development Project (2018YFB2001203).

✉ Ruilong Du
durl@zhejianglab.com

✉ Sumian Song
songsm@zhejianglab.com

✉ Haihui Yuan
yuanhh@zhejianglab.com

✉ Hua Zhou
hzhou@zju.edu.cn

[1] State Key Laboratory of Fluid Power and Mechatronic Systems, Zhejiang University, Hangzhou 310027, China

[2] Intelligent Robot Research Center, Zhejiang Lab, Hangzhou, China

[3] Department of Automation, Tsinghua University, Beijing, China

[4] Department of Electrical Engineering, Dalhousie University, Halifax, Nova Scotia, Canada

firstly interpolate the joint angle trajectories by splines or polynomials; then analyzes the walking behavior leveraging the dynamic parameters of the robot [2]. The other would analyze the walking behavior directly using a simplified model, among which the linear inverted pendulum (LIP) model characterized a concentrated mass above and a massless leg below, was the most commonly used; then the joint angle trajectories could be acquired by inverse kinematics [3].

Using these concepts, many biped robots have been constructed, trying to implement the biped's dynamic locomotion, such as Asimo [4], Walker-man [5], Walker [6], and the biped robot built in our earlier work [7], and et al. [8]. Common to these robots' leg configurations is that the leg is taken as a mechatronic system pursuing the goal of obtaining mechanical structures with higher strength, joint drives with higher power density, and control systems with higher bandwidth [9, 10]. With regard to the leg's stiffness, it is typically hoped that the stiffness should be large enough since larger stiffness could reduce the legs' deflection during movement, thus improving the control accuracy of the joint angle trajectories [11, 12]. However, in addition to a mechatronic system, the biped robot is characterized by a legged terrestrial locomotion base, whose legs take turns to be the swinging leg and the standing leg. By switching from the swinging phase to the standing phase, a great impact could be observed when the foot touches down to the ground, causing several unfavorable aspects to the biped robot [13]. Firstly, great energy loss would be observed since the velocity component of the swinging leg normal to the ground had to come to a sudden stop. Secondly, a great impact pulse would be generated due to the sudden stop, which might cause damages to the robot's structures, reducers and motors. Thirdly, the sudden stop would alter the continuous state of the leg's movement and the impact pulse could be taken as a disturbance to the robot, which inevitably added to the difficulty of the stability control of the biped, in particular when travelling on uneven terrains [14].

Biological biped systems, such as humans, birds, et al., inspire a promising design concept for biped robots that can overcome the aforementioned unfavorable aspects [15]. This is due to the excellent locomotion performance of biological bipedal systems that can be observed in everyday life, i.e., energy-efficient walking, less prone to injuries, and excellent dynamic locomotion behavior. With regard to the bio-inspired design concept, Seyfarth et al. studied the basic dynamics of human walking and running [16], and Daley et al. focused on the bipedal locomotion of striding ground birds [17]. An intriguing common aspect to their research findings is that the biological biped locomotion dynamics behave in a spring-like way and the legs could be taken as compliant elements, regardless of humans or birds [18]. To explain the biological biped's spring-like walking behavior, a spring-loaded inverted pendulum (SLIP) model was proposed, which was characterized by a concentrated mass above and a massless spring below, and could be mathematically modelled like a spring-mass system [19].

Previous research has demonstrated that the compliance of the leg plays a crucial role in the SLIP model for the biped's spring-like walking, and lots of efforts could be seen putting to the implementation of the leg's compliance. Generally speaking, two main strategies could be seen in the previous works to realize compliance, i.e., active compliance and passive compliance. In terms of active compliance, the leg configuration could maintain the same as those biped robots that were built based on the LIP model, except for the adding of sensing units for force or torque, such as joint torque sensors for electrically driven robots, fluid pressure sensors for hydraulically driven robots [20]. This is because the sensing information of forces or moments in contact with the ground needs to be fed back so as to achieve compliance via active control approaches, such as impedance control [21], force-position hybrid control [22], et al. As a result, realizing active control would inevitably add to the complexity of the control approach, and more energy was needed to maintain joint angle trajectories to match SLIP model. In terms of passive compliance, elastic elements, such as springs or leaf springs, will be added to the leg configuration, and the compliance of the leg is passively determined by the properties of the elastic elements. Utilizing the concept of passive compliance, several biped robots with different leg morphologies, capable of dynamic and efficient locomotion, were constructed [23, 24].

Despite different morphologies, these robots share two main features that are consistent with the SLIP model, the majority of mass concentrated over the thighs or waist, and the compliant leg structure via the introduction of elastic elements. In some academic studies, the exact morphology of the SLIP model was directly utilized, where a linear guided spring was put at the distal end and a point mass was put above, just like a pogo stick or clock-actuated SLIP. However, these leg configurations cannot work in the same way as articulated legs, thus limiting their practical applications in general human-built environments [25–27]. Some leg configurations adopted typical series articulated configuration, using series elastic actuators (SEA) for joints' drive to implement the SLIP behavior. However, the joint's spring in series usually played a role as a second-order low-pass filter on the high-frequency dynamics, thus limiting the bandwidth of the control system [28–30]. Lee et al. proposed a biarticular mechanism using SEAs, where the control bandwidth could somehow be improved via parameters optimization of the biarticular mechanism [31]. Luo et al. designed a biped robot driven by series elastic hydraulic actuators to implement the SLIP-based control and realized spring-like locomotion [32]. Nils et al. built a robot RAMone driven by high compliance series elastic actuators to exploit the natural dynamics of biped locomotion [33]. Ames et al. developed a robot DURUS by placing springs in the shanks [34].

In 2015, Hurst et al. developed a biped robot Atrias adopting a parallel and antagonistic mechanism in the leg. Two parallel motors were placed above and two leaf springs in series with the motors were placed in the lower leg [35]. The leg configuration of Atrias was quite a successful design that approximated the SLIP model and enabled robust locomotion over the unstructured ground. However, the two parallel motors would do antagonistic work during walking, thus casing unnecessarily power dissipation and power requirements. Noticing this flaw, Hurst et al. developed a new biped robot Cassie with two serial motor joints, a hip motor and a knee motor, which enabled the leg to swing strictly by the hip motor, thus avoiding doing antagonistic work [36]. It is worth noting that the knee motor joint, together with five other joints, including two spring joints and three passive joints, forms a compliant six-bar linkage mechanism. Such a leg configuration proves successful for spring-like walking and meets the practical need of collapsibility like other articulated legs [37].

By introducing a compliant six-bar linkage mechanism, the leg's kinematics and dynamics which would largely influence the performance of the spring-like walking, are inevitably growing much more complicated and desperately worth discussing. However, with regard to the publications of this particular leg configuration, most of them addressed the issues of spring-like gait panning, and related control strategies [38–40]. Few publications could be found on discussing the compliant mechanism of the leg configuration, in particular the stiffness of the leg, which was one of the most important parameters in the spring-mass system, i.e. the SLIP model. Xiong et al. discussed a derivation of the leg stiffness based on the motion of the spring joints and the motor joints. However, Xiong's work mainly focused on the jumping or walking control of the biped, while factors affecting the leg stiffness were not discussed from the perspective of the leg configuration [41, 42].

Furthermore, regarding the SLIP model, it should be noted that although the SLIP model takes the leg as a massless spring, it is not feasible in the actual leg configuration design since legs inevitably have mass in the actual configuration. In the case of a massed leg, impact and energy loss would still occur when touching down to the ground, though the leg is spring-loaded. Karssen et al. discussed the impact effect for optimizing the swing-leg retraction rate for running with respect to a kneed leg configuration [43, 44]. To the best of the authors' knowledge, few publications could be found discussing the influence of the mass of the leg regarding the leg configuration with a compliant six-bar linkage mechanism.

In this work, a biped's compliant leg as shown in Fig. 1, which was comprised of two serial motors and a compliant six-bar linkage mechanism, was developed and analyzed. Regarding the spring-like walking via utilizing the passive compliance of the leg, it is expected that when the leg touches the ground and gets into the standing phase, it would firstly be compressed just like a spring; and then it would return to its original length (the relaxed length). By designing the walking gait, the leg leaves the ground and gets into the swing phase when the leg returns to its original length. Therefore, it is crucial to investigate the stiffness and the dynamic characteristics of the compliant leg, which would be analyzed theoretically and experimentally in this work with respect to a jumping motion. The jumping motion covers both the standing phase and the flying phase, and would have characteristics similar to those of spring-like walking, thus contributing to the understanding of spring-like walking. The main contributions of this work can be summarized as: 1) a compliant leg is proposed and the relation between its kinematics and stiffness is presented; 2) the influence of the mass of the leg is accounted for to analyze the dynamic characteristics of the leg; 3) an algorithm for the leg's jumping is presented taking the leg's mass into consideration.

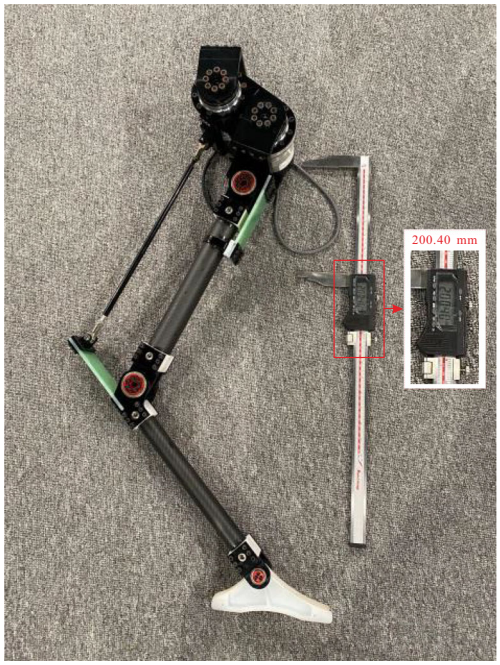

Fig. 1 Current leg configuration of our compliant leg design

The rest of this work is organized as follows. In section 2, a detailed description of the leg configuration is presented, and after that, a numerical model is introduced on the kinematics and stiffness of the leg. Section 3 depicts the dynamic modelling of the compliant leg and the algorithm for jumping planning taking the leg's mass into account. Section 4 brings the numerical results and discussions on the kinematics, stiffness and dynamic characteristics of the leg. Section 5 introduces the experiment setup and related experimental verification results. After that, Section 6 presents the conclusions and the future work.

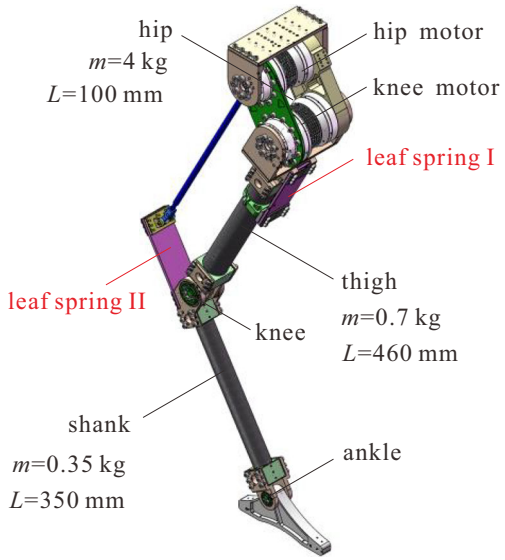

Fig. 2 The CAD model of the designed compliant leg

2 Design and Modelling the Compliant Leg

2.1 Structural Design of the Leg

Figure 2 presents the CAD model of the designed compliant leg in this work, whose dimension is based on human leg proportions, with the height being able to reach around 900 mm under full extension and 300 mm under full contraction. The leg mainly consists of three parts: a hip with two serial actuated motors, a thigh composed of a compliant linkage mechanism by leverage of two leaf springs, and a shank connected with an underactuated foot.

To satisfy the SLIP model and further to satisfy the biped robot's spring-like walking behavior, the two serial motors implement the leg's swinging and contraction; and the compliant linkage mechanism implements the leg's spring-like behavior. The leaf springs are made of the same material with elasticity and their geometric parameters are carefully matched. The underactuated foot is adopted to increase the contact area with the ground, compared to the point-footed configuration. The underactuated foot is connected to the shank through a rolling bearing, and thus, it can rotate around the ankle freely. To avoid the foot sole flipping over during the jumping phase, a sponge strip is stuffed into the ankle joint to prevent excessive rotation of the foot when it leaves the ground.

According to the design principle of the SLIP model, most of the mass is concentrated in the hip thanks to the two heavy motors. Additionally, extra load can be put above the hip, so as to further increase the ratio of the mass above the spring leg. To ensure the lightweight and sufficient strength of the leg, the hip structure uses aluminum alloy material while the thigh and the shank use carbon fiber and POM materials. It is worth mentioning that, to investigate the leg's mass on its dynamic characteristics, additional weights could be attached to the ankle or the knee joint to alter the leg's mass.

2.2 Kinematics and Stiffness Modelling

The leg's kinematics and stiffness are of prior concern in order to implement the spring-like walking behavior. As shown in Fig. 3, a kinematic analysis schematic for the designed leg is presented. As observed, three types of joints are presented: purple for the actuated motor joint, yellow for the spring joint and green for the passive joint. With regard to the kinematics, the foot's position F (x_F, y_F) relative to the hip position M (x_M, y_M), which denotes the leg's length and the swinging angle (L, θ), is of particular concern. Putting point M as the origin, with the known geometric parameters of the lengths of the linkages (L_{MN}, L_{NP}, …), and the known initial angles of the spring joints (θ_P, θ_Q), all the joints' positions X(x, y) can be determined by four parameters (θ_M, θ_N, δ_P, δ_Q)

$$X = f\left(\theta_M, \theta_N, \delta_P, \delta_Q\right) \tag{1}$$

where θ_M and θ_N denote the rotation angles of the motors M and N. δ_P and δ_Q denote the deflection angles of the spring joints P and Q.

As shown in Fig. 3(a), the rotation angle of motor M is defined as the angle between the vertical direction and the linkage MN; the rotation angle of motor N is defined as the angle between the linkage MN and the linkage NP. The positive directions of the motors are shown by the red arrows.

Judging from Eq. (1), to obtain the kinematics, the deflection angles of the spring joints need to be determined first. As shown in Fig. 3(b) is the layout of the spring joint P. In the actual layout, the joint P is a passive revolute joint in parallel with a leaf spring which can be taken as a cantilever beam with a length l. Putting a force F_{can} to the end of the leaf spring, a deflection Δd_{can} can be seen at the end of the leaf spring, which would result in the same displacement of the thigh, as shown in Fig. 3(c). Hence, the passive joint P can be taken as a spring joint as shown in Fig. 3(d), which would undergo a deflection of δ_P under a torque M. And the stiffness of the spring joint P can be evaluated as:

$$k_P = \frac{M}{\delta_P} = \frac{F{\cdot}l}{\Delta d_{can}/l} = \frac{F{\cdot}l^2}{\left(F{\cdot}l^3\right)/(3EI)} = \frac{3EI}{l} \tag{2}$$

where E denotes the elastic modulus of the leaf spring; I denotes the cross-sectional moment of inertia of the leaf spring; l denotes the length of the leaf spring. The stiffness of the spring joint Q can be defined in the same way.

As shown in Fig. 4, when forces F_x and F_y are acting on the foot, deflections of the spring joints P and Q (δ_P, δ_Q), as well as a displacement of the foot (Δx, Δy), are expected. Via force

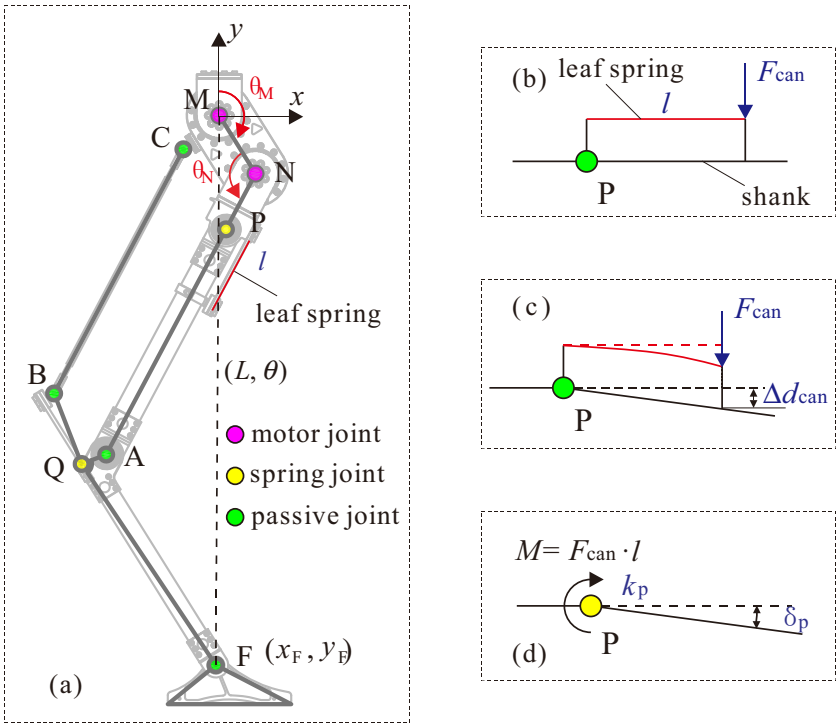

Fig. 3 Kinematics diagram and spring joints analysis of the leg

analysis of the leg configuration, several momentum balance equations for the joints can be derived.

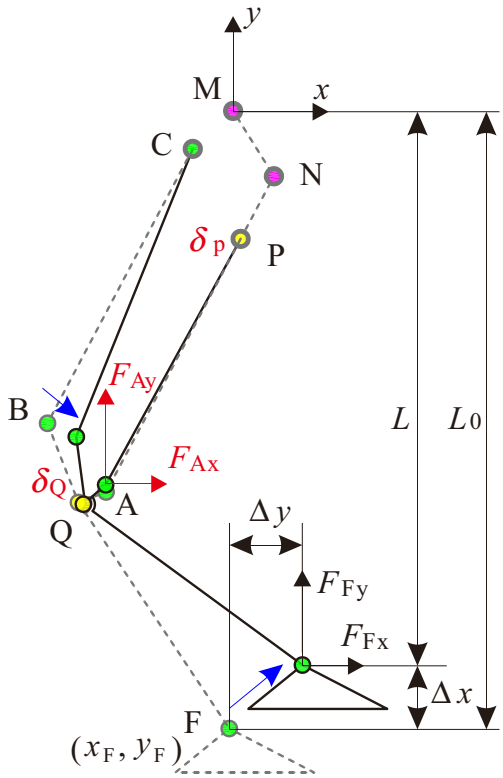

Fig. 4 Deflection of the leg due to forces applied on the foot

For the spring joint P:

$$\mathbf{F}_{\mathrm{A}}^{(\mathrm{AP})} \times \mathbf{r}_{\mathrm{PA}} + k_{\mathrm{p}} \cdot \boldsymbol{\delta}_{\mathrm{P}} = 0 \tag{3}$$

For the spring joint Q:

$$\mathbf{F}_{\mathrm{A}}^{(\mathrm{AQ})} \times \mathbf{r}_{\mathrm{QA}} + \mathbf{F}_{\mathrm{F}}^{(\mathrm{FQ})} \times \mathbf{r}_{\mathrm{QF}} + k_{\mathrm{Q}} \cdot \boldsymbol{\delta}_{\mathrm{Q}} = 0 \tag{4}$$

where

$$\mathbf{F}_{\mathrm{A}}^{(\mathrm{AP})} = -\mathbf{F}_{\mathrm{A}}^{(\mathrm{AQ})} \tag{5}$$

For the passive joint B:

$$\mathbf{F}_{\mathrm{Q}}^{(\mathrm{QB})} \times \mathbf{r}_{\mathrm{BQ}} + k_{\mathrm{Q}} \cdot \boldsymbol{\delta}_{\mathrm{Q}} = 0 \tag{6}$$

where

$$\mathbf{F}_{\mathrm{Q}}^{(\mathrm{QB})} = \mathbf{F}_{\mathrm{F}}^{(\mathrm{FQ})} + \mathbf{F}_{\mathrm{A}}^{(\mathrm{AQ})} \tag{7}$$

For the passive joint C

$$\mathbf{F}_{\mathrm{B}}^{(\mathrm{BC})} \times \mathbf{r}_{\mathrm{CB}} = 0 \tag{8}$$

where

$$\mathbf{F}_{\mathrm{B}}^{(\mathrm{BC})} = \mathbf{F}_{\mathrm{Q}}^{(\mathrm{QB})} \tag{9}$$

In Eqs. (3)–(9), vector **F** denotes the force vector, where the subscript denotes the point of the force acting on, and the

superscript denotes the linkage to which the force acts; vector **r** denotes the linkage vector.

Judging from Eq.s (3) (4) (6) and (8), it can be seen that they form a system of nonlinear equations that includes four unknown variables $(\delta_p, \delta_Q, F_{Ax}^{AP}, F_{Ay}^{AP})$. Hence, it can be numerically solved using Newton's iterative method (converged to 10^{-8}).

After getting the deflection of the spring joints δ_P and δ_Q, the kinematics of the legs could be achieved, including the foot's new position thanks to forces F_x and F_y. Hence, the resultant displacement of the foot $(\Delta x, \Delta y)$ shown in Fig. 4 could be calculated; and the stiffness of the leg can be determined as:

$$\begin{bmatrix} k_x & k_{xy} \\ k_{yx} & k_y \end{bmatrix} \cdot \begin{bmatrix} \Delta x \\ \Delta y \end{bmatrix} = \begin{bmatrix} F_x \\ F_y \end{bmatrix} \tag{10}$$

where k_x and k_y denote the unidirectional stiffness in x and y directions, respectively; k_{xy} and k_{yx} denote the stiffness in mixing directions.

According to the SLIP model, the leg's stiffness denotes the stiffness in y direction. Moreover, when the leg is only subjected to a vertical force F_y ($F_x = 0$), only the deformation in the y-direction is desired and no deformation in the x-direction is desired. By optimizing the stiffness of the spring joints P and Q, the value of Δx could be minimized when subjected to only the vertical forces F_y ($F_x = 0$); and thus, the leg's vertical stiffness could be evaluated by Eq. (11). This work mainly focuses on the vertical characteristics of the leg, and therefore the leg's vertical stiffness is also referred to as the leg's stiffness in the rest of this work.

$$k = F_y/\Delta y \tag{11}$$

3 Dynamic Modelling of the Compliant Leg

3.1 Modified Spring-Mass Model of the Leg

After getting the stiffness of the leg, a modified spring-mass model can be utilized to investigate the dynamic characteristics of the leg, as shown in Fig. 5, where m_1 denotes the mass concentrated on the hip; m_2 denotes the mass of the leg; k denotes the stiffness of the leg; and c denotes the damper of the leg induced by the friction of the joint bearings, et al.

With respect to the motion phases of a single leg, it can be divided into two types: the flying phase in the air and the standing phase on the ground. This work is focused on the vertical jumping motion of the leg, and its related two phases are shown in Fig. 6: the vertical flying phase and the vertical standing phase. Using the modified spring-mass model, the motion equation for the vertical jumping can be expressed as:

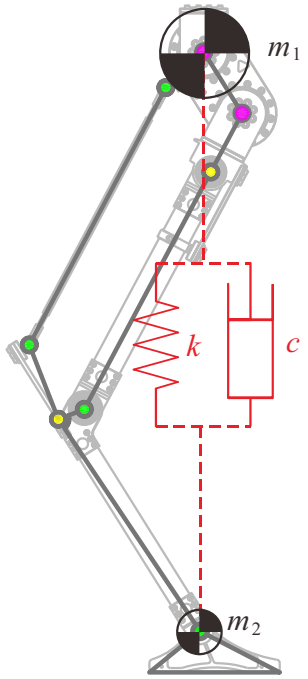

Fig. 5 Modified spring-mass model for the designed compliant leg

$$\begin{bmatrix} m_1 & 0 \\ 0 & m_2 \end{bmatrix} \cdot \begin{bmatrix} \ddot{h}_1 \\ \ddot{h}_2 \end{bmatrix} + \begin{bmatrix} c & -c \\ -c & c \end{bmatrix} \cdot \begin{bmatrix} \dot{h}_1 & \dot{h}_2 \end{bmatrix} + \begin{bmatrix} k & -k \\ -k & k \end{bmatrix} \cdot \begin{bmatrix} h_1 \\ h_2 \end{bmatrix} + \begin{bmatrix} m_1 g - kL_s \\ m_2 g + kL_s - F_c \end{bmatrix} = 0 \tag{12}$$

where L_s denotes the relaxed length of the spring; F_c denotes the contact force between mass m_2 and the ground, i.e. the contact force between the foot and the ground.

Regarding the vertical flying phase, as shown in Fig. 6(a), mass m_1 and m_2 are in the air with $F_c = 0$. Regarding the vertical standing phase, as shown in Fig. 6(b), mass m_2 is on the ground with $h_2 = 0$ and $\dot{h}_2 = 0$.

As for the switch from the flying phase to the standing phase, the judging criteria can be described as:

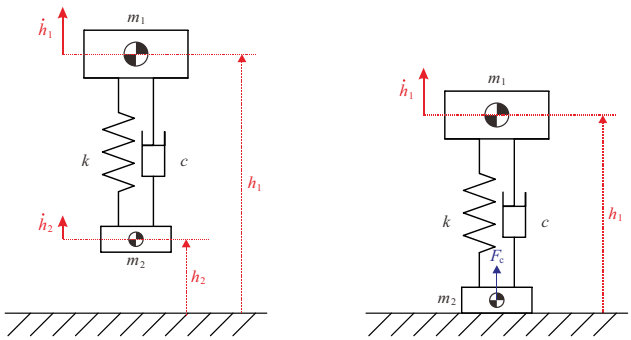

(a) vertical flying phase (b) vertical standing phase

Fig. 6 Two motion phases with respect to the vertical jumping motion. (a) vertical flying phase (b) vertical standing phase

$$\left\{h_2^- > 0 \& h_2^+ = 0\right\} \tag{13}$$

As for the switch from the standing phase to the flying phase, the judging criteria can be described as:

$$\left\{F_c^- > 0 \& F_c^+ = 0 \& \dot{h}_1^{+} > 0\right\} \tag{14}$$

where the superscript - denotes the case prior to a certain moment, and the superscript + denotes the case after a certain moment.

Impact with the ground would occur as it switches from the flying phase to the standing phase, since the mass of the leg is accounted for. The impact was taken as fully inelastic impact, i.e. the velocity of mass m_2 came to a sudden zero at the switching moment, and the energy loss could be evaluated as:

$$E_{\text{loss}}^{(\text{imp})} = \frac{1}{2} m_2 \cdot \dot{h}_2^2 \tag{15}$$

Using the modified spring-mass model, the force acting on the hip refers to the force arising from the spring and the damper, which is directly related to the torque of motors M and N, can be evaluated as:

$$F_{\text{up}} = k(h_1 - h_2 - L_s) + c\left(\dot{h}_1 - \dot{h}_2\right) \tag{16}$$

3.2 Algorithm for Vertical Jumping Planning

Judging from the kinematics modelling in Eq. (1), the relaxed length of the spring L_s denotes the relaxed length of the leg with deflections of the spring joints $\delta_P = 0$ and $\delta_Q = 0$. Hence, the relaxed length of the spring is determined by the rotation angles of motors M and N, and can be described as:

$$L_s = g(\theta_M, \theta_N) \tag{17}$$

Fig. 7 presents the jumping up process via the motor joint actuation from the initial static standing phase.

The spring leg is subjected to a compressed deflection s with respect to a relaxed length L_s, and an equation can be obtained as follows:

$$L_s = h_1 + s \tag{18}$$

The jumping up process ends followed by switching into the flying phase, which is judged by Eq. (14). Take the relaxed length L_s as a polynomial on time t:

$$L_s = \alpha_0 + \alpha_1 \cdot t + \alpha_2 \cdot t^2 + \alpha_3 \cdot t^3 + \alpha_4 \cdot t^4 + \alpha_5 \cdot t^5 + \alpha_6 \cdot t^6 \tag{19}$$

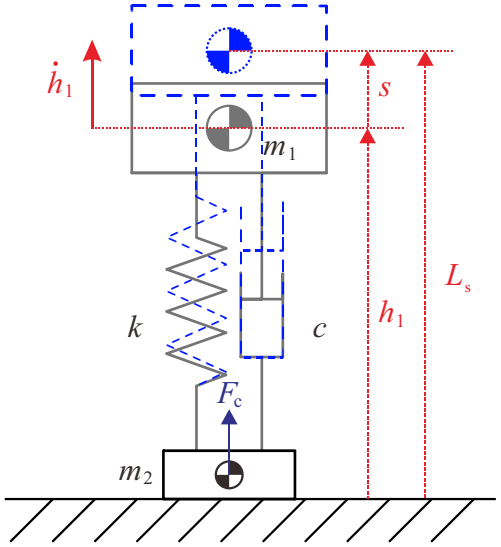

Fig. 7 Jumping up process via the motor joint actuation from the initial standing phase

which is subjected to

$$\begin{cases} L_s|_{t=t_0} = \alpha_0 = L_{\text{ini}} \\ L_s \in (L_{\min}, L_{\max}) \\ \dot{L}_s|_{t=t_0} = \alpha_1 = 0 \end{cases} \tag{20}$$

where L_{ini} denotes the initial relaxed length of the leg; $L_{\min}$ and $L_{\max}$ denote the minimum and maximum relaxed length of the leg that could be arrived at via motor joint actuation, respectively; and $[\alpha_0, \alpha_1, \alpha_2, \alpha_3, \alpha_4, \alpha_5, \alpha_6]^T$ denotes the parameters to be optimized for a specific purpose of the jumping up process, such as the minimum time for the jumping up process, the maximum velocity $\dot{h}_1$ at the switching moment, et al.

After obtaining the optimized parameters for α, the trajectory of the relaxed length of the leg can be achieved and the motor joint angle trajectories can be obtained via inverse kinematics using Eq. (16). Then the jumping process could be implemented via a position control strategy of motors M and N.

4 Simulation Results and Discussion

4.1 Kinematic Analysis

The length of the linkages of the leg depicted in Fig. 3 is provided in Table 1.

Figure 8 demonstrates the leg's swinging from the perspective of kinematic analysis using MATLAB modelling. As observed, motor N would stay standstill, and the leg's swinging could be implemented by only rotating motor M. As

Table 1 Length of the linkages of the leg

linkage	length (mm)	linkage	length (mm)
MN	100.00	NP	92.00
PA	372.00	AQ	38.35
QB	110.42	BC	402.90
CM	71.88	QF	352.61

shown by the red dashed line, the leg swinging is characterized by the foot travelling at a circle centered at motor M, which suggests that the leg length remains the same as the leg swings. More importantly, a one-to-one linear relationship between the rotation angle of motor M and the leg's swinging angle could be observed, which makes it easy to control the leg swinging in the SLIP model.

The leg's contraction could be implemented by only rotating motor N. However, motor M also needs to be rotated in order to remain the leg's swinging angle constant, as shown in Fig. 9. By rotating motors N and M, the leg can be contracted from around 900 mm to 300 mm, featuring vertical movement of the foot, thus enabling control of the leg length in the SLIP model. As shown in Fig. 10, a two-to-one linear relationship could be seen between the rotation angles of motor N and motor M, with the purpose of easily controlling the vertical contraction of the leg. As shown by the blue line in Fig. 10, the leg length extends from 300 mm to 900 mm as motor N rotates from 40° to 160°, and the contraction rate lowered as the leg length increases. Between 600 mm and 800 mm, which is the typical leg length range for walking, motor N rotates from 80° to 120°, and the contraction rate lies at around 5 mm/°.

4.2 Stiffness Analysis

Figure 11 demonstrates the leg's deflection due to a vertical force F_y with respect to different relaxed leg lengths. The blue circle denotes the relaxed state of the leg while the red circle denotes the deflection state under a 300 N vertical force F_y. As observed, the positions of motors N and M remain unchanged

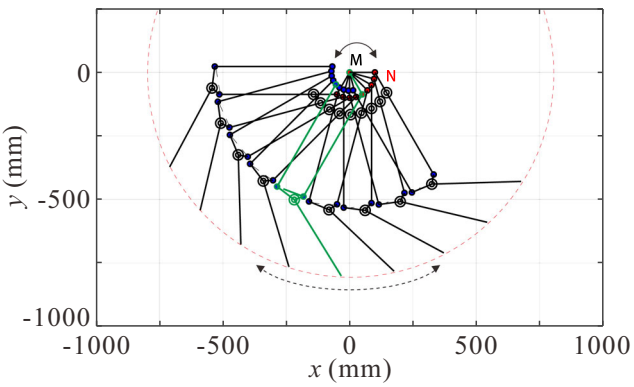

Fig. 8 Kinematic demonstration of the leg swinging

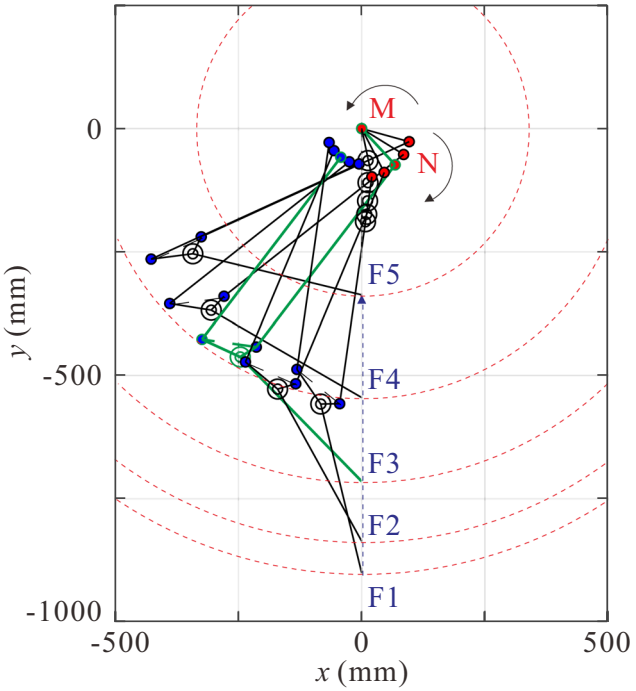

Fig. 9 Kinematic demonstration of the leg contraction

while the spring joints deflect to resist the vertical force, leading to a deflection of the lower leg. This is favorable for the SLIP model-based control since the lower leg has a small mass and behaves like a spring. Two cases of the relaxed leg lengths were displayed by changing the rotation angle of motor N. As shown by the adjacent blue and red circles, a greater deflection could be seen for the case of shorter initial leg length, indicating that the stiffness decreases as the relaxed leg length becomes smaller.

Figure 12 depicts the values of Δx and Δy when the foot is subjected to a vertical force F_y. As seen, the ratio of Δy to Δx is greater than 10, and the ratio could be seen rapidly rising as θ_N increases (the leg length increases), suggesting the deformation in the x direction can be ignored when only the vertical force is applied. For a certain relaxed leg length, Δy increases as the loading force increases, which is in accordance with the behavior of a spring. Additionally, for a certain loading force, the value of Δy could be seen growing as the rotation angle decreases (the relaxed leg length decreases), suggesting a

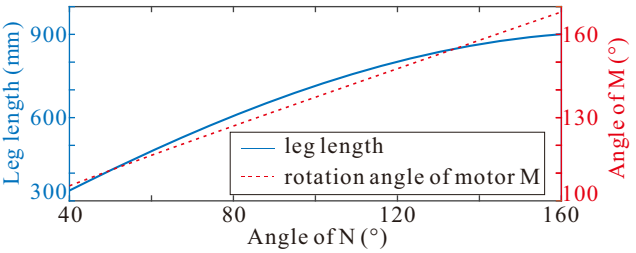

Fig. 10 Angle relations between the hip motor and knee motor for the leg contraction

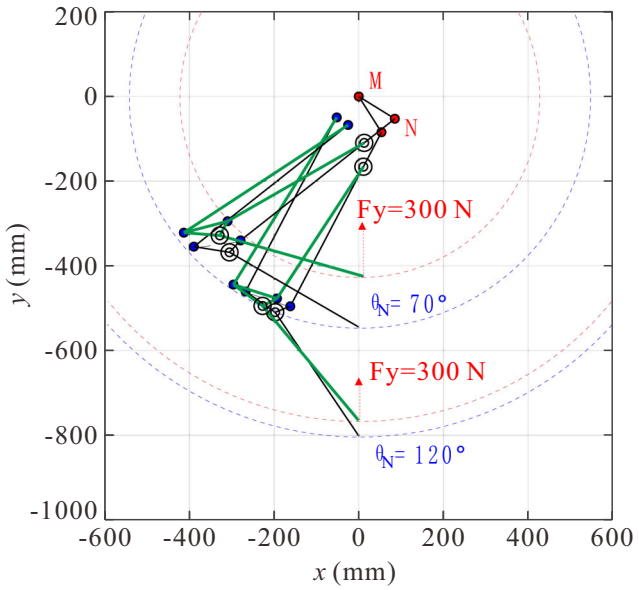

Fig. 11 Demonstration of the leg deflection due to vertical forces *F*y with respect to different leg lengths

rather interesting phenomenon, namely that the stiffness of the designed leg increases with increasing leg length.

Figure 13 depicts multiple curves of the leg stiffness regarding different rotation angles of motor N ranging from 60° to 130°, and the relaxed leg length from around 450 mm to 850 mm. For a curve related to a certain rotation angle, the rightmost point of the curve refers to the relaxed length of the leg. As observed, as the loading force increases, the leg length decreases due to the leg being compressed, and the stiffness of the leg is getting smaller as well. It is worth noting that despite the different relaxed lengths of the legs (different curves), their stiffness values and the paths of becoming smaller remain very well in agreement, which suggests that the stiffness of the legs is much more related to the length of the legs and less related to the relaxed length of the legs. Noting this, the stiffness of the leg can be approximated by a polynomial relating the length of the leg, as shown by the red fitting curve:

$$k = \beta_0 + \beta_1 \cdot L + \beta_2 \cdot L^2 + \beta_3 \cdot L^3 + \beta_4 \cdot L^4 \tag{21}$$

where β_x is the polynomial parameter.

4.3 Dynamic Performance under Different Leg Mass and Stiffness

To investigate the dynamic characteristics of the leg with respect to different mass and stiffness, the leg was lifted to a height of 0.1 m, and then dropped. In this subsection, the dynamic performance of the leg's dropping was evaluated using MATLAB simulation.

Fig. 14 depicts the leg's dynamic performance regarding different leg mass (m_1 = 10 kg, k = 8000 N/m, c = 0). It can be seen that when the leg is taken as massless (0.001 kg), the trajectories of m_1 and m_2 exhibit periodical patterns and they can climb up to the same maximum height in the following

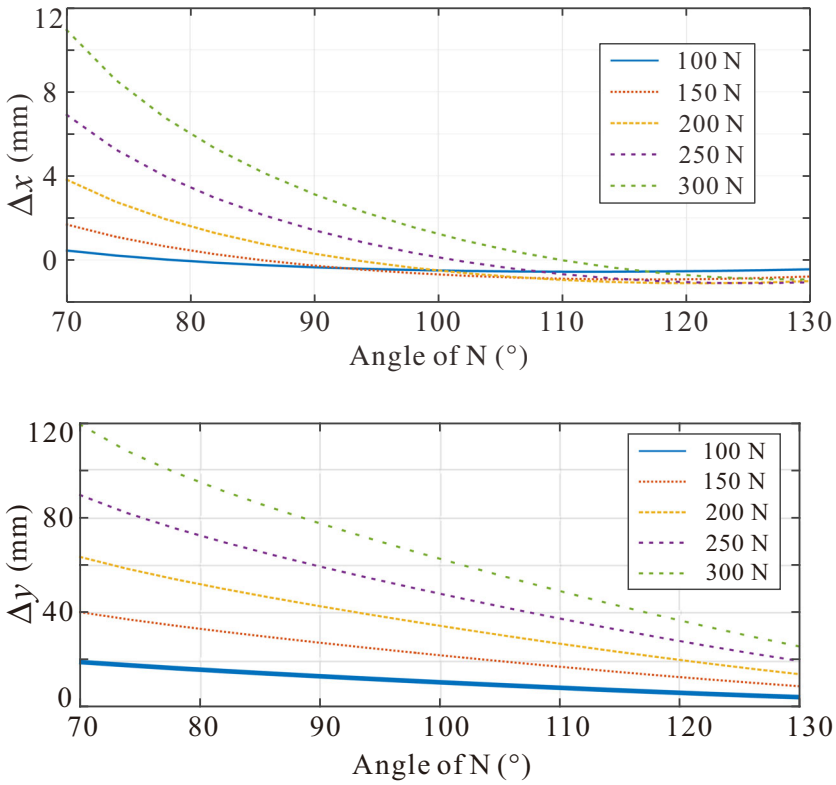

Fig. 12 Δx and Δy when subjected to a vertical force F_y

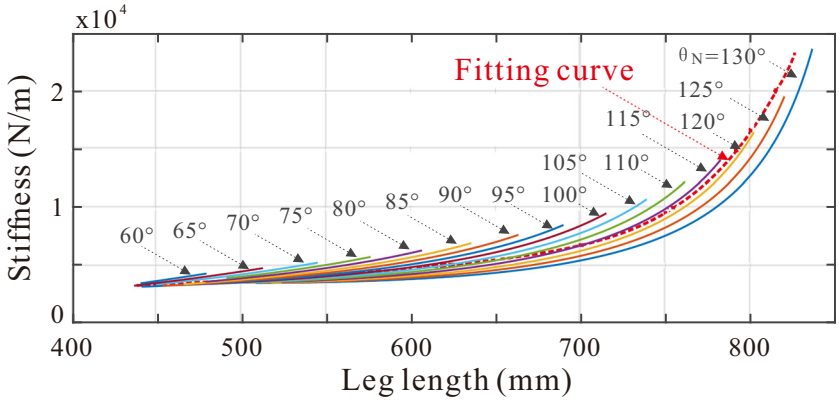

Fig. 13 Leg stiffness with respect to different leg lengths

flying phase, since there is no energy loss at touchdown. As the leg mass grows, the maximum height of the flying phase becomes smaller, due to a greater energy loss induced by the impact according to Eq. (15). As for the force acting on the hip, as the leg mass grows, no significant increase could be seen during the standing phase while a significant increase could be observed during the flying phase. It suggests that as the leg mass grows, higher and varying torque is required for motors M and N during the flying phase, which is an unfavorable aspect from the point of view of energy consumption, and a more unfavorable aspect from the perspective of motion control of the leg.

With regard to the biped's spring-like walking, the swinging phase of the leg refers to the flying phase here. The requirement of higher and varying torque on the motor would inevitably add to the difficulty of controlling the swinging leg, leading to greater errors when the leg touches the ground, such as the touchdown location, the leg length at the touchdown moment, et al., which would certainly further affect the performance of the standing phase and the biped's walking.

The maximum height of the first flying phase in Fig. 14 is of particular interest for the biped's spring-like walking. Define two ratios λ and ε as shown in Eq. (22), the first of which is the mass of the leg to the mass concentrated in the hip, and the second of which is the maximum height in the first flying phase to the initial dropping height:

$$\begin{cases} \lambda = m_2/m_1 \\ \varepsilon = \left(h_{\mathrm{f,max}} - h_{\mathrm{s,min}}\right)/\left(h_{\mathrm{ini}} - h_{\mathrm{s,min}}\right) \end{cases} \tag{22}$$

Fig. 15 depicts the relations of two defined ratios λ and ε. It can be seen that ε decreases from 1 as λ increases from 0,

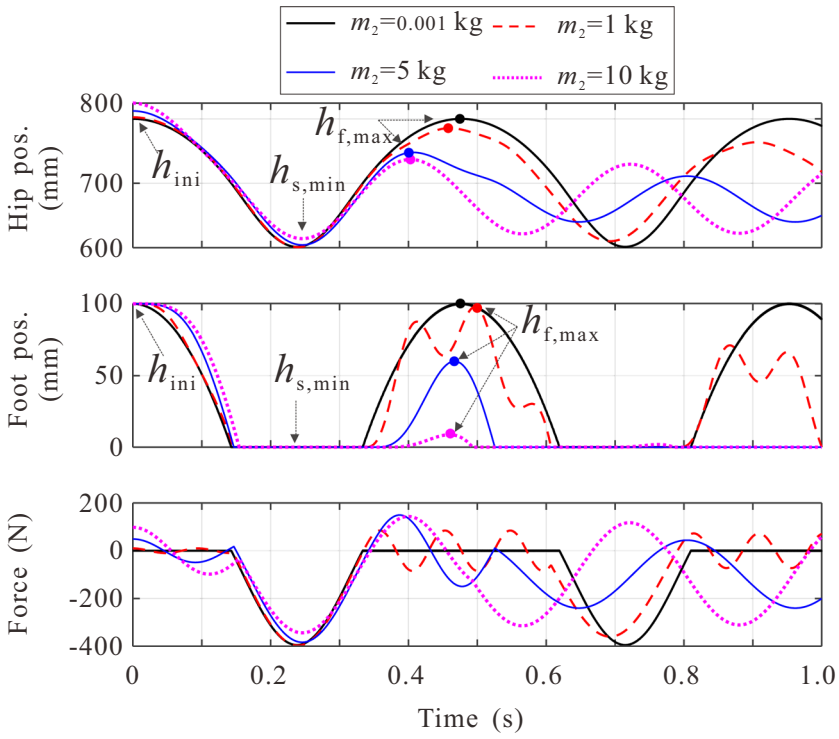

Fig. 14 Dynamic performance regarding different leg mass

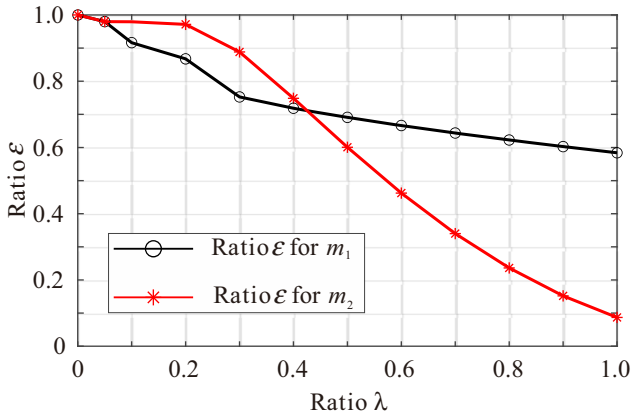

Fig. 15 Relations of two define ratios for presenting the influence of the leg's mass

demonstrating the unfavorable aspect of the mass of the leg. It can also be seen that ε_1 for m_1 could reach up to 0.9 when λ is less than 0.1, while it would decrease sharply when λ is greater than 0.1. This suggests that the leg mass should be maintained below one-tenth of the mass concentrated in the hip when designing the leg for spring-like walking.

Fig. 16 depicts the leg's dynamic performance regarding different leg stiffness (m_1 = 10 kg, m_2 = 1 kg, c = 0). No significant difference could be seen in the maximum height of the flying phase, as the stiffness changes. However, earlier arrival of the maximum height can be observed as the stiffness increases. This is mainly because the time spent in the standing phase is considerably shorter, which is defined by the intrinsic frequency of the typical spring-mass system during the standing phase in Eq. (23). It suggests that a higher step frequency for a higher travelling speed could be realized by increasing the leg's stiffness when performing a spring-like walking. According to.

Eq. (21), this could be satisfied by increasing the leg length. As for the force acting on the hip, a significant increase could be observed in the standing phase as the stiffness increases, demanding higher torque of motors M and N. The greater the leg length, the higher the leg stiffness, the faster the step frequency, and the greater the motor torque required.

$$\omega = \sqrt{k/m_1} \tag{23}$$

4.4 Dynamic Performance of Vertical Jumping

Fig. 17 depicts the dynamic performance of the leg's vertical jumping using MATLAB simulation. It can be seen that the hip's location is lower than the leg length due to the compression of the spring-loaded leg at the initial moment. During the jumping up process, motors M and N rotate to ensure that the leg extends vertically, as shown by the blue solid line. The difference between the hip position and the leg length is progressively increasing and then diminishing, and the final hip position catches up with the leg length. This is because the mass concentrated on the hip needs to accelerate upward first to ensure that the jumping speed is obtained, thus requiring a greater spring force. As a result, a greater leg compression can be observed in the first place. After it has gained sufficient

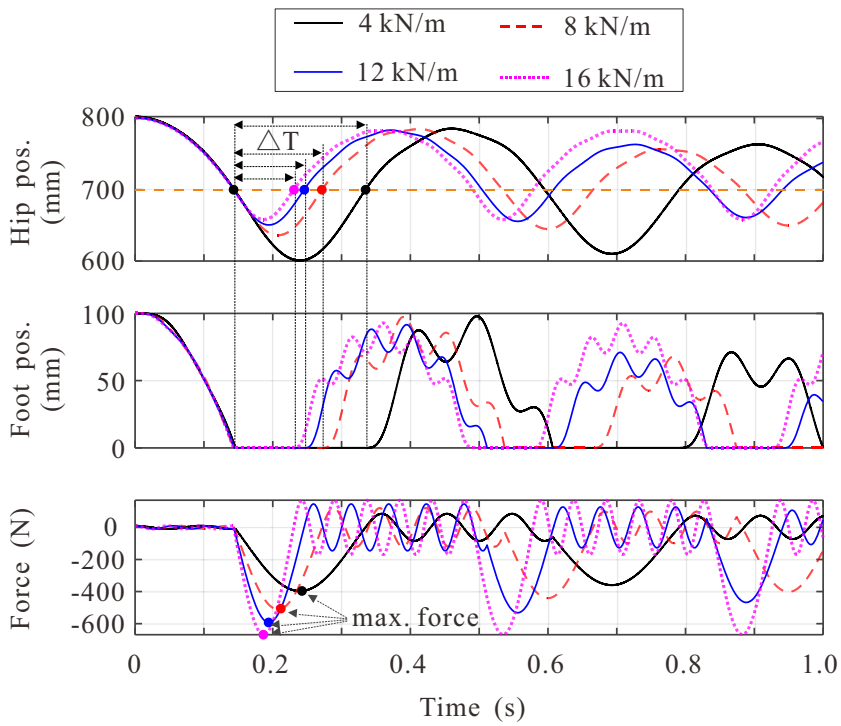

Fig. 16 Dynamic performance regarding different leg stiffness

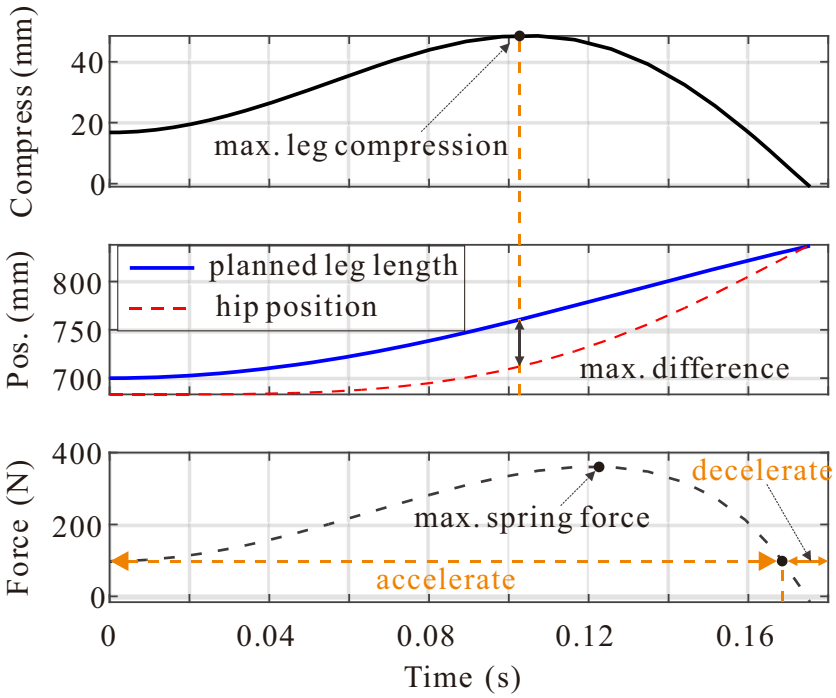

Fig. 17 Dynamic performance of the leg's vertical jumping

velocity, it needs to decelerate to make the contact force between the foot and the ground zero, thus satisfying the jumping condition defined by Eq. (14). It is worth noting that the curve of the spring force and the leg compression do not exactly coincide because the leg is a variable stiffness spring, the longer the leg, the greater the stiffness. It is also worth noting that the compression length of the leg is not reduced to a zero, but to a negative value, namely in an extended condition, because it takes the mass of the leg into account.

5 Experimental Verification

5.1 Experimental Setup

In order to validate the analysis on the leg's stiffness and its dynamics, experiments were conducted on the designed leg configuration with the experiment set up displayed in Fig. 18. As observed, the upper end of the leg (the hip) was connected to a guiding plate which could only move up and down along the guide bar. The total weight of the guiding plate and the mass concentrated above was around 100 N, and the leg was around 10 N. Additional weights could be added on the guiding plate for increasing the loading force; and additional weights could be added to the ankle for increasing the mass of the leg, as well. The other end of the leg (the foot) was standing on the ground, supporting the weight of the leg, the guide plate and additional weights. Two displacement sensors (effective scale: 0–1500 mm and 0–350 mm; accuracy: 0.5% FS) were placed on the ground for measuring the displacement of the foot and the hip. The two motors are the same as each other, with rated voltage 48 V, sample time 1 ms, maximum torque 60 Nm, and maximum speed 60 rpm. The sample rate of sensors was set to 1 kHz.

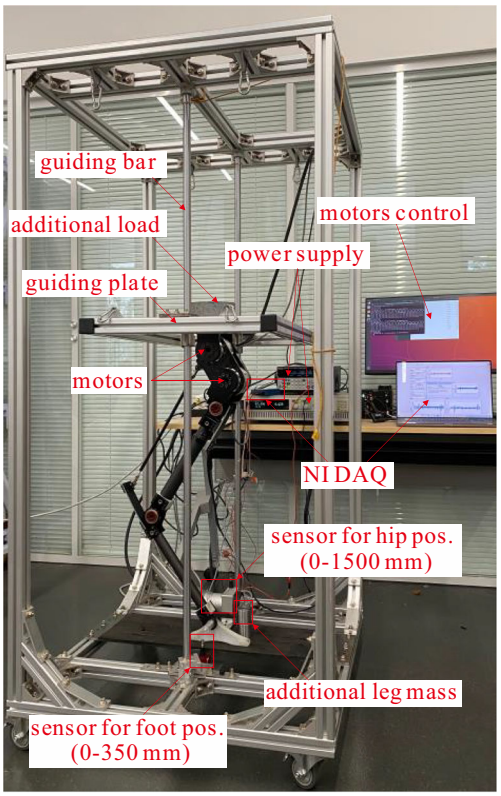

Fig. 18 Experiment setup for measuring the leg's stiffness and jumping height

5.2 Experiments on Stiffness

To verify the model on the stiffness of the leg, a loading experiment was conducted for measuring the stiffness. Figure 19 depicts the experimental data with respect to different leg lengths and vertical loading forces. The data in the red box was the relaxed length of the leg, and the leg length could be observed to getting reduced as the loading force increased, consistent with the spring-like behavior. Moreover, it could be seen that the measured leg length (shown by the black stars) was in good agreement with that obtained from the stiffness model (shown by blue line), validating the stiffness model. Apart from that, straight lines were displayed as well (the red dotted line), which connected the data referring to 0 N and 300 N. Both the experimental data and the data from the model could be seen in the right-hand side of the straight lines, validating the characteristic of variable stiffness, the longer the leg, the higher the stiffness.

5.3 Experiments on Dropping

To verify the influence of the mass and the stiffness of the leg, a dropping experiment was conducted via dropping the leg from a height of 0.1 m, and then measuring the displacement of the foot and the hip. The mass of the leg could be increased via adding additional weights to the ankle, as shown in Fig. 18; and the stiffness of the leg could be changed via adjusting the leg length. Figure 20 depicts the experimental data for dropping the leg with respect to different leg masses. As observed, as the mass of the leg rising, the maximum height of the flying phase is decreasing. Particularly in the case of 4 kg, there is almost no significant flying phase, thus justifying the influence of the leg's mass. Basically, only one flying phase could be observed, which was believed to be due to the damper

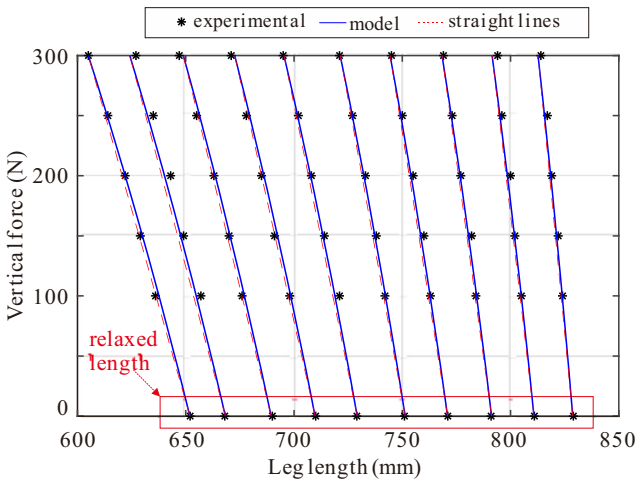

Fig. 19 Experimental data with respect to different leg length and vertical force

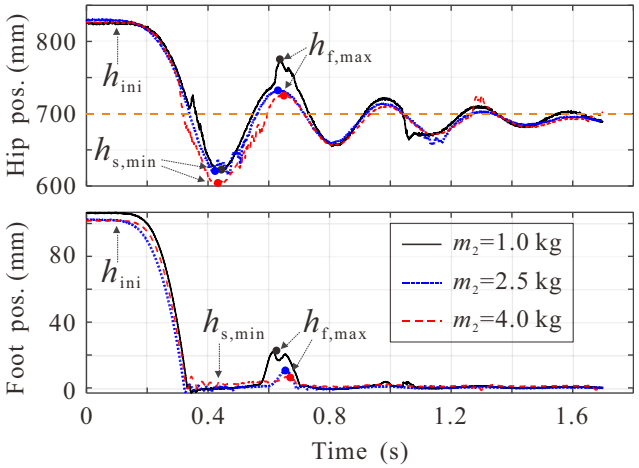

Fig. 20 Experimental data for dropping with respect to different leg mass

of the leg and the friction between guiding plate and the guide bar, leading to a greater energy loss.

Fig. 21 depicts the experimental data with respect to different stiffness of the leg. The black curves represent the experimental dropping data for the shorter leg with smaller stiffness; the red curves represent the experimental dropping data for the longer leg with greater stiffness. As the stiffness increases, the arrival of the maximum height in the flying phase could be seen arriving earlier, consistent with the analysis in Eq. (23). By understanding this dynamic feature and experimentally verifying it, the step frequency for the biped's spring-like walking could be changed via adjusting the length of the leg to change the travelling speed.

5.4 Experiments on Jumping

Figure 22 depicts the experimental data for a single vertical jump and its related snapshots. The initially planned relaxed length of the leg was 700 mm, while the initial height of the hip could be observed around 685 mm, which was believed to be due to the compression of the leg due to the mass concentrated on the hip. It switched to the flying phase after a vertical jumping up process which took around 0.17 s. At the switching moment, the leg length was around 837 mm, which was around 1 mm longer than the planned relaxed length of the leg, and this was believed to be because of the mass of the leg. The maximum jumping height in the flying phase was around 150 mm, followed by several flying phases after the leg touched down to the ground again. The final length of the leg was around 826 mm after it had stopped moving up and down. The compression of the leg was 15 mm when the relaxed length of the leg was 700 mm at the initial state, and 10 mm when the relaxed length of the leg was 836 mm at the final state. This justifies the characteristic of variable stiffness of the leg, and the planning algorithm for the vertical jumping, as well.

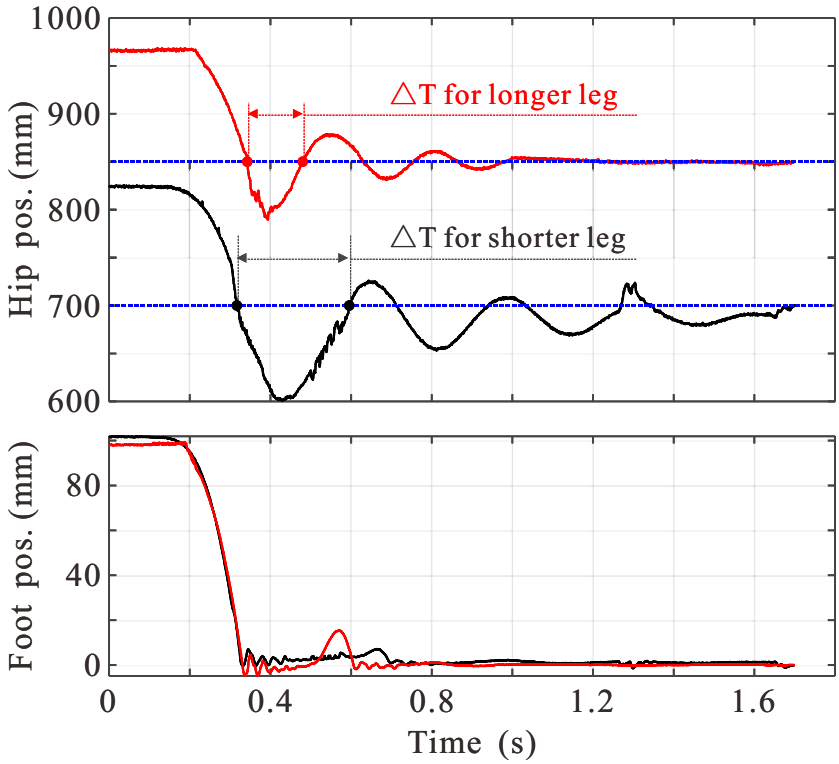

Fig. 21 Experimental data for dropping with respect to different stiffness

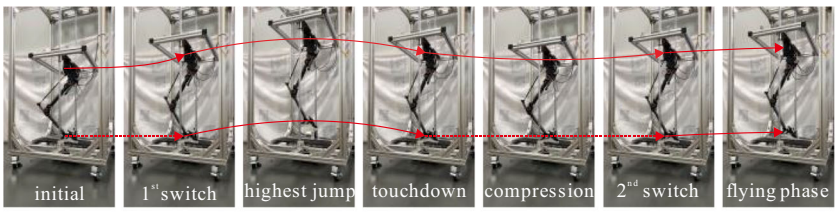

(a) snapshots for a single jump

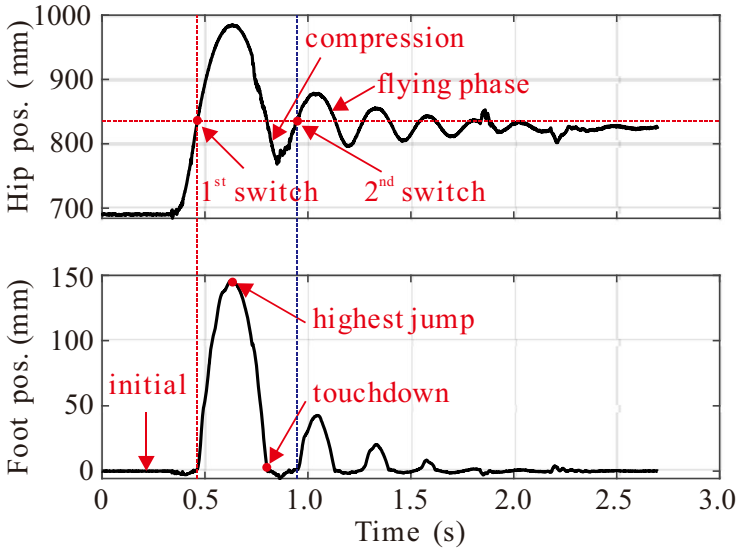

(b) experimental data for the single jump

Fig. 22 Experimental results on a single jump of the leg. (a) snapshots for a single jump. (b) experimental data for the single jump

The leg could perform consecutive jumps by squatting after touching the ground, and then stretching to jump up again, as depicted in Fig. 23. As observed, it could jump higher by squatting to a lower position in order to gain more elastic potential energy in the spring leg, as shown in the red box. Apart from that, periodical consecutive jumps could be performed as well, as shown in the blue box. This demonstrates the feasibility of the leg performing the biped's spring-like walking, regardless of moving periodically at a certain step frequency and speed, or at different speeds by changing the step frequency or the step size.

6 Conclusion

In this work, a compliant leg configuration capable of implementing spring-like walking for a biped robot was presented. Numerical models were introduced to analyze the stiffness and the dynamic characteristics of the leg, taking the leg's mass into account.

Simulation results showed that the leg could be taken as a variable stiffness spring with respect to the length of the leg, the longer the leg, the greater the stiffness. Furthermore, it suggested that the mass of the leg should be maintained below one-tenth of the mass concentrated in the hip for spring-like walking. Apart from that, the dynamic analysis suggested that a greater stiffness of the leg could lead to a faster step frequency for spring-like walking, thus enabling different travelling speed via adjusting the length of the leg.

Experiments were conducted to verify the numerical model and the dynamic analysis. Experiments on the stiffness of the leg showed a good agreement with the stiffness calculated by the presented numerical model, and the experiment in which the leg was dropped from a certain height justified the dynamic analysis of the leg. Afterwards, experiments were conducted on single vertical jumps and consecutive jumps of the leg respectively, demonstrating the feasibility of the leg to perform the biped's spring-like walking, regardless of a certain speed, or different speeds by changing the step frequency or the step size.

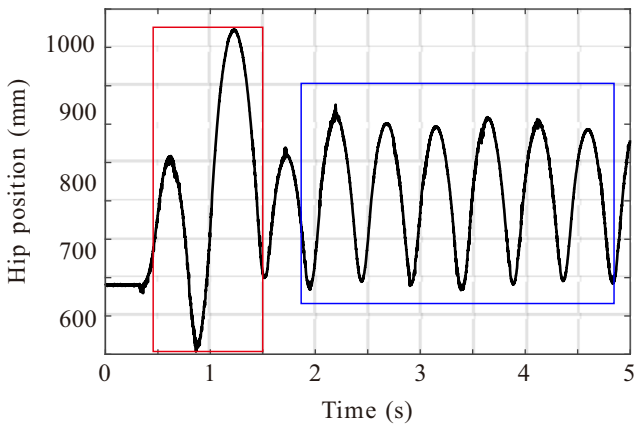

Fig. 23 Experimental data for consecutive jumps

In the next step, a biped robot will be constructed with two compliant legs presented in this work, to implement planar spring-like walking for biped robots. In the long term, a 3D biped robot featuring spring-like walking will be built with the ability to travel in real human-built environments.

Authors' Contributions Guifu Luo and Ruilong Du designed the study, performed the research, analyzed data, and wrote the paper. They contributed equally to this work.

Shiqiang Zhu contributed to the design of the test rig, helped performed the analysis with constructive discussions.

Sumian Song and Haihui Yuan wrote and debugged the code, helped conduct the experiment and analyze data.

Hua Zhou contributed to the manuscript preparation, helped perform the analysis with constructive discussions.

Mingguo Zhao and Jason Gu contributed to the improvement of the manuscript quality, helped perform the analysis with constructive discussions.

Funding This work was supported by NSFC Project (No. 51905495, No.51821093, No.51890885), the China Postdoctoral Project (No. 2020 M671821), NSF Project of Zhejiang Province (No. LQ20E050009, No. LQ21F030003), and the National Key Research and Development Project (2018YFB2001203).

Declarations

Conflict of Interest The authors have no conflicts of interest to declare that are relevant to the content of this article.

Code or Data Availability Not applicable.

Ethics Approval Not applicable.

Consent to Participate Not applicable.

Consent for Publication All authors consent to publish their work in this journal.

References

1. Raibert, M.: Legged Robots that Balance. MIT press Cambridge, MA (1986)
2. Chevallereau, C., Westervelt, E.R., Grizzle, J.W.: Asymptotically stable running for a five-link, four-actuator, planar bipedal robot. Int. J. Rob. Res. **24**(6), 431–464 (2005)
3. Kajita S., Kanehiro F., Kaneko K., Yokoi K., Hirukawa H.: The 3D linear inverted pendulum mode: A simple modeling for a biped walking pattern generation. In: Proceedings of the IEEE/RSJ International Conference on Intelligent Robots and Systems. Expanding the Societal Role of Robotics in the the Next Millennium, Maui, pp. 239–246(2001)
4. Shigemi, S., Goswami, A., & Vadakkepat, P.: ASIMO and humanoid robot research at Honda, Humanoid robotics: A reference. Springer, pp. 55–90(2019)
5. Tsagarakis, N.G., Caldwell, D.G., Negrello, F., et al.: Walk-man: A high-performance humanoid platform for realistic environments. J. Field. Robot. **34**(7), 1225–1259 (2017)

6. Zhang R., Zhao M., Wang C.L.:Standing push recovery based on LIPM dynamics control for biped humanoid robot In: 2018 IEEE International Conference on Robotics and Biomimetics (ROBIO), Kuala Lumpur, pp. 1732–1737(2018)
7. Yuan, H., Song, S., Du, R., et al.: A Capturability-based Control Framework for the Underactuated Bipedal Walking. In 2021 IEEE International Conference on Robotics and Automation (ICRA), pp. 6804–6810(2021)
8. Hereid, A., Hubicki, C.M., Cousineau, E.A., Ames, A.D.: Dynamic humanoid locomotion: A scalable formulation for HZD gait optimization. IEEE T Robot. **34**(2), 370–387 (2018)
9. Kaneko, K., Kaminaga, H., Sakaguchi, T., et al.: Humanoid robot HRP-5P: An electrically actuated humanoid robot with high-power and wide-range joints. IEEE Robot. Autom. Lett. **4**(2), 1431–1438 (2019)
10. Kuindersma S., Permenter F., Tedrake R.: An efficiently solvable quadratic program for stabilizing dynamic locomotion. In: 2014 IEEE International Conference on Robotics and Automation (ICRA), Hong Kong, pp. 2589–2594(2014)
11. Lohmeier S.: Design and realization of a humanoid robot for fast and autonomous bipedal locomotion. Ph.D. thesis, Technische Universität München, 2010
12. Park, I.-W., Kim, J.-Y., Lee, J., Oh, J.-H.: Mechanical design of the humanoid robot platform. HUBO. Adv. Robot. **21**(11), 1305–1322 (2007)
13. Wang Z., He B., Shen R., Meng W.: Contact impact inhibition strategy for biped robot walking based on central pattern generator. In: 2015 IEEE International Conference on Robotics and Biomimetics (ROBIO), Zhuhai, pp. 733–738(2015)
14. Seleem I.A., Assal S. F. M., Mohamed A. M.: Cyclic gait planning and control of underactuated five-link biped robot during single support and impact phases for normal walking. In: 2018 IEEE International Conference on Industrial Technology (ICIT), Lyon, pp. 123–128(2018)
15. Hubicki, C., Abate, A., Clary, P., et al.: Walking and running with passive compliance: Lessons from engineering: A live demonstration of the ATRIAS biped. IEEE Robot. Autom. Lett. **25**(3), 23–39 (2018)
16. Seyfarth, A., Geyer, H., Günther, M., et al.: A movement criterion for running. J. Biomech. **35**(5), 649–655 (2002)
17. Daley, M.A.: Understanding the agility of running birds: sensorimotor and mechanical factors in avian bipedal locomotion. Integr. Comp. Biol. **58**(5), 884–893 (2018)
18. Geyer, H., Seyfarth, A., Blickhan, R.: Compliant leg behaviour explains basic dynamics of walking and running. Proc. R. Soc. B. **273**, 2861–2867(2006) (1603)
19. Geyer, H., Seyfarth, A., Blickhan, R.: Spring-mass running: simple approximate solution and application to gait stability. J. Theor. Biol. **232**(3), 315–328 (2005)
20. Liu Y., Wensing P. M., Schmiedeler J. P., et al.: Terrain-blind humanoid walking based on a 3-D actuated dual-SLIP model. IEEE Robot. Autom. Lett. 1(2), 1073–1080(2016)
21. Fan Y., Li X., Feng H., et al.: Compliance Control of the Hydraulic-Driven Single Legged Robot. In: 2019 IEEE International Conference on Robotics and Biomimetics (ROBIO), Dali, pp. 2117–2122(2019)
22. Lee, H.J., Kim, J.Y.: Balance control strategy of biped walking robot SUBO-1 based on force-position hybrid control. Int. J. Precis. Eng. **22**(1), 161–175 (2021)
23. Reher J., Cousineau E.A., Hereid A., et al.: Realizing dynamic and efficient bipedal locomotion on the humanoid robot DURUS. In: 2016 IEEE International Conference on Robotics and Automation (ICRA), Stockholm, pp. 1794–1801(2016)
24. Hubicki, C., Grimes, J., Jones, M., et al.: Atrias: Design and validation of a tether-free 3d-capable spring-mass bipedal robot. Int. J. Rob. Res. **35**(12), 1497–1521 (2016)
25. Joe, H.M., Oh, J.H.: A robust balance-control framework for the terrain-blind bipedal walking of a humanoid robot on unknown and uneven terrain. Sensors. **19**(19), 4194 (2019)
26. Bledt, G., Powell, M. J., Katz, B., Di Carlo, J., Wensing, P. M., & Kim, S.: MIT Cheetah 3: Design and control of a robust, dynamic quadruped robot. In 2018 IEEE/RSJ International Conference on Intelligent Robots and Systems (IROS), pp. 2245–2252 (2018)
27. Gao, H., Liu, Y., Ding, L., et al.: Low impact force and energy consumption motion planning for hexapod robot with passive compliant ankles. J. Intell. Robot. Syst. **94**(2), 349–370 (2019)
28. Manara, S., GianMaria, G., Garabini, M., Caporale, D., Gabiccini, M., Bicchi, A.: Analysis of series elasticity in locomotion of a planar bipedal robot. Int. J. Mech. Control. **20**(11), 1–9 (2019)
29. Maiorino, A., Muscolo, G.G.: Biped robots with compliant joints for walking and running performance growing. Front. Mech. Eng. **6**(11), 1–11 (2020)
30. Sarkar, A., Dutta, A.: Optimal trajectory generation and design of an 8-dof compliant biped robot for walk on inclined ground. J. Intell. Robot. Syst. **94**(3), 583–602 (2019)
31. Lee, C., Oh, S.: Development, analysis, and control of series elastic actuator-driven robot leg. Front. Neurorobot. **13**(17), 1–31 (2019)
32. Luo, J., Wang, S., Zhao, Y., Fu, Y.: Variable stiffness control of series elastic actuated biped locomotion. Intell. Serv. Robot. **11**(3), 225–235 (2018)
33. Smit-Anseeuw, N., Gleason, R., Vasudevan, R., Remy, C.D.: The energetic benefit of robotic gait selection—a case study on the robot RAMone. IEEE Robot. Autom. Lett. **2**(2), 1124–1131 (2017)
34. Ma, W. L., Kolathaya, S., Ambrose, E. R., et al.: Bipedal robotic running with DURUS-2D: Bridging the gap between theory and experiment. In Proceedings of the 20th international conference on hybrid systems: computation and control, pp. 265–274(2017)
35. Grimes, J. A., and Hurst J. W.: The design of ATRIAS 1.0 a unique monopod, hopping robot. Adaptive Mobile Robotics. 548–554(2012)
36. Abate, A.M.: Mechanical design for robot locomotion. Ph.D. thesis, School of Mechanical, Industrial, and Manufacturing Engineering. Oregon State University, USA (2018)
37. "Cassie - Next Generation Robot", https://www.youtube.com/watch?v=Is4JZqhAy-M
38. Gong Y., Grizzle J.: One-step ahead prediction of angular momentum about the contact point for control of bipedal locomotion: Validation in a lip-inspired controller. In: 2021 IEEE International Conference on Robotics and Automation (ICRA), 2021
39. Green K., Hatton R.L, Hurst J. W.: Planning for the unexpected: Explicitly optimizing motions for ground uncertainty in running. In: 2020 IEEE International Conference on Robotics and Automation (ICRA), Paris, pp. 1445–1451(2020)
40. Apgar, T., Clary, P., Green, K., Fern, A., & Hurst, J. W.: Fast Online Trajectory Optimization for the Bipedal Robot Cassie. In Robotics: Science and Systems, Pittsburgh, 101(14) (2018)
41. Xiong X., Ames A. D.: Bipedal hopping: Reduced-order model embedding via optimization-based control. In: 2018 IEEE/RSJ International Conference on Intelligent Robots and Systems (IROS), Madrid, pp. 3821–3828(2018)
42. Xiong X., Ames A.D.: Coupling reduced order models via feedback control for 3d underactuated bipedal robotic walking. In: 2018 IEEE-RAS 18th International Conference on Humanoid Robots (Humanoids), Beijing, pp. 67–74(2018)
43. Karssen, J.G.D., Haberland, M., Wisse, M., et al.: The effects of swing-leg retraction on running performance: analysis, simulation, and experiment. Robotica. **33**(10), 2137–2155 (2015)
44. Karssen J. G. D., Haberland M., Wisse M., et al.: The optimal swing-leg retraction rate for running. In: 2011 IEEE International Conference on Robotics and Automation, Shanghai, pp. 4000–4006(2011)

Guifu Luo received the B.S. degree in the College of Mechanical and Electrical Engineering from Central South University, Changsha, China, in 2018, and he is currently a Ph.D. candidate in the State Key Laboratory of Fluid Power and Mechatronic Systems, School of Mechanical Engineering, Zhejiang University, Hangzhou, China.

His research interests include electro-hydraulic system control, dynamics modelling and control of biped robots.

Ruilong Du received the B.S. degree and the Ph.D. degree in mechatronic engineering from Zhejiang University, China, in 2012 and 2018, respectively. He is currently a Postdoctoral Research Fellow with the Zhejiang Lab and the Department of Automation, Tsinghua University.

His research interests include mechanical design of biped robots, electro-hydraulic system control, and hydraulic components.

Shiqiang Zhu received his Ph.D. degree in mechatronic control from Zhejiang University. He is a full professor and doctoral advisor at Zhejiang University. He is also President of Zhejiang Lab and Vice President of Zhejiang University, as well as a member of the expert panel of "Intelligent Robot", a national key R&D program. Meanwhile, he is also Chairman of Zhejiang Robot Industry Association, and Chairman of Zhejiang Artificial Intelligence Industry Alliance (AIIA).

He has long been dedicated to exploring intelligent robot and intelligent systems. While focusing on intelligent robot, he has also had in-depth study of intelligent home service robot, exoskeleton robot, machine vision, high-performance multi-axis motion controller, electromechanical hydraulic automatic control system, and construction of robot standard system.

He has published over 200 papers in authoritative journals home and abroad, and he is a main responsible person for developing industry standards, including 2 for China's robotics industry and 1 for International Electrotechnical Commission (IEC). He has also obtained more than 70 national invention patents, many of which have already been commercialized.

Sumian Song received the B.S. degree and the Ph.D. degree in electrical engineering from Zhejiang University, China, in 2013 and 2018, respectively. He is currently a research fellow at Zhejiang Lab.

His research interests include motion control of biped robots, nonlinear system and reinforcement learning.

Haihui Yuan received the B.S. degree from School of Mechanical Engineering and Automation, Northeastern University, China, in 2012, the Ph.D. degree in School of Mechanical Engineering, Zhejiang University, China, in 2018. He is currently an assistant researcher in Zhejiang Lab.

His research interest focuses on the gait planning and control of biped robots.

Hua Zhou received the B.Eng., M.Eng., and Ph.D. degrees in mechanical engineering from Huazhong University of Science and Technology, Wuhan, China, in 1990, 1993, and 1998, respectively. He is currently a Professor in the Department of Mechanical Engineering, Zhejiang University, Hangzhou, China.

His research interests include water hydraulic component and system development, electro-hydraulic system control, and ship hydraulics and its vibration reduction and noise reduction. He has been rewarded with the Second Class of the National Scientific and Technological Progress Award, and the First Class of the Chinese Universities Technological Award.

Mingguo Zhao received his B.E., M.Sc. and Ph.D. degrees from Harbin Institute of Technology in 1995, 1997 and 2001 respectively. From 2001 to2003, he held a postdoctoral position in the Department of Precision Instrument, Tsinghua University. He is currently a Professor of Department of Automation, Tsinghua University.

His current research interests include biped locomotion control and Whole-Body Control of hyper-redundant robots.

Jason Gu received the bachelor's degree in electrical engineering and information science from the University of Science and Technology of China, in 1992, the master's degree in biomedical engineering from Shanghai Jiao Tong University in 1995, and the Ph.D. degree from the University of Alberta, Canada, in 2001.

He is currently a Full Professor of Electrical and Computer Engineering with Dalhousie University, Canada. He is also a Cross-Appointed Professor with the School of Biomedical Engineering for his multidisciplinary research work. He has over 24 years of research and teaching experience and has authored over 350 conference papers and articles.

His research areas include robotics, biomedical engineering, rehabilitation engineering, neural networks, and control. He is a fellow of the Engineering Institute of Canada and Canada Academy of Engineering. He has been the Associate Editor of the Journal of Control and Intelligent Systems, Transactions of the Canadian Society for Mechanical Engineering, Canada, the IEEE Transactions on Mechatronics, the International Journal of Robotics and Automation, Unmanned Systems, the Journal of Engineering and Emerging Technologies, and the IEEE Access.

Dr. Gu is currently IEEE Canada President for 2020–2021.